Complex Principal Component Analysis: Theory and Examples

J. D. HOREL

Climate Research Group, Scripps Institution of Oceanography, University of California, San Diego, La Jolla, CA 92093

(Manuscript received 14 March 1984, in final form 25 September 1984)

ABSTRACT

Complex principal component (CPC) analysis is shown to be a useful method for identifying traveling and standing waves in geophysical data sets. Combinations of simple progressive and standing oscillations are used to examine the properties of this technique. These examples illustrate that although CPC analysis allows for the identification of traveling waves, many of the drawbacks associated with conventional principal component analysis remain, and sometimes become worse; e.g. the interpretation of CPC solutions is more difficult since both amplitude and phase relationships must be considered. A method for linearly transforming complex principal components was devised in order to identify regional relationships within large geophysical data sets. The errors in CPC analysis resulting from limited sample sizes are discussed.

1. Introduction

Many geophysical phenomena derive from interactions between traveling waves of different spatial scales and temporal frequencies. Cross-spectral analysis is the most widely accepted method for studying such phenomena (e.g., Kao, 1968; Madden and Julian, 1971; Hayashi, 1973; Hayashi, 1979; Speth and Madden, 1983). However, it is difficult to use cross-spectral analysis in an exploratory fashion when the dominant frequencies and spatial scales are unknown. Also, cross-spectral analysis is less informative when it is applied to regional, nonstationary phenomena characterized by short lived, irregularly occurring episodes, as is the case in many climatic fluctuations.

Principal component (PC) analysis has been widely used to explore the spatial and temporal relationships within large geophysical data sets. The primary advantage of the PC approach is its ability to compress the complicated variability of the original data set into the fewest possible number of modes. However, conventional PC analysis detects standing oscillations only, not traveling waves.

Principal component analysis has been extended in several ways in order to detect propagating phenomena. Weare and Nasstrom (1982) determined the eigenvectors of lagged covariance matrices which were derived from observations sampled at a limited number of successive time steps. Since this approach becomes extremely expensive in computer time as the number of time steps (lags) is increased, it can only resolve propagating phenomena over a limited time span.

Certain special cases such as unidirectional progressive Poincaré waves [i.e. waves for which pressure fields have solutions of the form $\mathrm{Re}[e^{i(x-t)}]$ can be detected by treating the zonal and meridional wind components as the real and imaginary parts of complex time series (Kundu and Allen, 1976; Hardy and Walton, 1978; Legler, 1983; Denbo and Allen, 1984). The complex cross-covariance matrices determined from such complex time series are decomposed into complex eigenvectors. This approach works only if the zonal and meridional wind components are nearly in quadrature. In the more general case of waves moving in more than one direction with pressure fields of the form $\mathrm{Re}[e^{i(x+y-t)}]$, the solutions derived from this approach may not detect the traveling waves.

Complex principal component analysis in the frequency domain (FDPC) was developed in a meteorological context by Wallace and Dickinson (1972) and subsequently used by Wallace (1972), Wang and Moers (1977), Hogg (1977), Michaelson (1982), and Venne (1984). This technique involves computing complex eigenvectors from cross-spectral matrices and it is described in detail in the text by Brillinger (1981). The FDPC approach is the most general of the available methods of studying propagating phenomena. Conventional PC analysis is simply FDPC analysis applied to contemporaneous data only. Because of its all encompassing nature, FDPC analysis may be cumbersome when applied to some climate-related problems. For example, if the power of a principal component is spread over a wide frequency band, then many maps (one for each spectral estimate) must be studied in order to document the phenomenon. Such situations arise if the climatic fluctuations occur at irregular intervals.

Complex principal component analysis in the time domain (hereafter referred to as CPC analysis) is an attractive alternative to FDPC analysis. It has been

applied to geophysical data sets by several investigators, e.g. Rasmusson *et al.* (1981), Barnett (1983, 1984a, 1984b), Anderson and Rosen (1983), and Trenberth and Shin (1984). Complex time series are formed from the original time series and their Hilbert transforms. Then, complex eigenvectors are determined from the cross-covariance or cross-correlation matrices derived from the complex time series. Complex principal component analysis is essentially FDPC analysis averaged over all frequency bands. In the extreme case where a data set is dominated by variability at one frequency only, then the FDPC and CPC techniques are identical (Brillinger, 1981, pg. 353). Hence, CPC analysis allows the efficient detection of propagating features, especially when the variance is spread over a number of frequencies. The CPC approach has considerable potential for being widely used to detect propagating phenomena. However, its basic properties have been incompletely documented and its limitations as an analysis technique have not been well explored.

Some of the characteristics of principal component techniques limit their usefulness for certain applications. These limitations include: spatial orthogonality of the spatial patterns, dependence of the solution on the domain of the analysis, difficulty in interpreting the solution when the number of variables is large, and the degeneracy of the solution when successive eigenvalues are nearly the same. These drawbacks have been discussed in detail by many investigators (e.g. Kutzbach, 1967, 1970; Barnett, 1977; Preisendorfer *et al.*, 1981; Walsh and Richman, 1981; Richman, 1981; Horel, 1981; and North *et al.*, 1982).

Experience with conventional PC analysis suggests that the PC technique can also be used to reduce the original data set into the fewest number of significant components (Harman, 1967; Walsh and Richman, 1981; Richman, 1981; Horel, 1981). Then, the components can be linearly transformed (rotated) in order to better fulfill the simple structure criterion of L. L. Thurstone (see Harman, 1967, pg. 98), and to yield a solution which suffers less from some of the aforementioned properties of principal components. One of the major advantages of such an approach is that strong regional relationships within large data sets can be emphasized. While the linear transformations of real principal components are thoroughly documented in textbooks (e.g. Harman, 1967), analogous ones for the case of complex principal components have not been developed.

Principal component analysis was used for many years before its inherent limitations were fully realized. The purpose of this paper is to demonstrate the basic properties of CPC analysis before this tool becomes widely used. The method of analysis is described in Section 2. Selected examples in Section 3 show the salient properties of the complex principal components and their transformations. A discussion of the sampling errors in CPC analysis follows in Section 4.

2. Method

Compared to the conventional principal component approach, the analysis procedure described in this paper contains two additional steps: one at the beginning and one at the end. First, the data field to be analyzed is augmented in a manner such that propagating features within it may be detected. The procedure used here is to derive a complex data matrix where the real part of the matrix is the original data field and the complex part is a data field with its phase, at every spectral frequency, shifted 90° from that of the original data field. The next step is to determine the eigenvalues and eigenvectors of the complex cross-correlation matrix. The complex principal components are computed from the data matrix and the eigenvectors. Finally, the complex principal components are recombined (rotated) according to the varimax criterion in order to obtain an alternative solution that emphasizes regional relationships within the data set. The theory behind these three steps is discussed in this section. Much of Sections 2a and 2b is based upon the paper of Barnett (1983). It is repeated here in order to expand upon several important points.

a. Generation of a complex data set

A scalar field $u_j(t)$, where j denotes spatial position and t is time, can be represented as

$$u_j(t) = \sum_{\omega} a_j(\omega)\cos\omega t + b_j(\omega)\sin(\omega t), \qquad (1)$$

where the Fourier coefficients (a, b) at positive frequency ω are defined in the usual manner. It is a common procedure to describe propagating features in terms of the complex representation of a variable:

$$U_j(t) = \sum_{\omega} c_j(\omega)e^{-i\omega t}, \qquad (2)$$

where $c_j(\omega) = a_j(\omega) + ib_j(\omega)$ and $i = \sqrt{-1}$. Expanding (2) using the definition of c_j yields

$$\begin{aligned} U_j(t) &= \sum_{\omega} [a_j(\omega)\cos(\omega t) + b_j(\omega)\sin(\omega t)] \\ &\quad + i[b_j(\omega)\cos(\omega t) - a_j(\omega)\sin(\omega t)] \\ &= u_j(t) + i\hat{u}_j(t). \end{aligned} \qquad (3)$$

The real part of (3) is simply the original data field. The imaginary part is called the quadrature function or Hilbert transform and it represents a filtering operation upon $u_j(t)$ in which the amplitude of each spectral component is unchanged but each component's phase is advanced by $\pi/2$ (Thomas, 1969).

In practice, an estimate of the Hilbert transform $\hat{u}_j(t)$ can be obtained directly from the Fourier coefficients of $u_j(t)$ derived from fast Fourier transform

(FFT) routines (for other approaches, see the paper by Barnett, 1983):

$$\hat{u}_j(t) = \sum_{\omega} W(\omega)[b_j(\omega)\cos(\omega t) - a_j(\omega)\sin(\omega t)] \quad (4)$$

and $W(\omega)$ is a filter weight at frequency ω. This approach is subject to the problems that normally attend Fourier analysis, e.g. aliasing, end effects, etc. Hilbert transforms obtained from FFT routines appear to be more strongly influenced by end effects than are the Fourier transforms themselves. Each end (roughly 10% of the total time series) should be tapered to eliminate this problem (see Madden and Julian, 1971). The researcher has the option of either studying the relationships among variables $U_j(t)$ summed over all frequencies [$W(\omega)$ equal to one for all ω] or restricting the summation to a range of frequencies $\omega_0 \pm \delta\omega$ [$W(\omega)$ equal to one near ω_0 and tapering to zero at $\omega_0 \pm \delta\omega$]. Of course, the original data $u_j(t)$ must also be passed through any filtering operation. The number of degrees of freedom in the spectral estimates depends on the nature of the filtering operator $W(\omega)$.

Figure 1 shows the Hilbert transforms of two extreme cases: a sine wave defined at a particular frequency and a pulse which contains energy at all frequencies. (For Hilbert transforms of other special functions see the text by Thomas, 1969.) In the first case, the Hilbert transform is simply the sine function shifted 90°. Figure 1b shows the complex time series $U(t) = u(t) + i\hat{u}(t)$ plotted in a vectorial format. Note that the amplitude of $U(t)$ is constant over time in this instance. It should also be recognized that since ω is defined at positive frequencies only, the phase of any complex time series can change in one direction only; it was arbitrarily chosen to be in the clockwise direction in this paper.

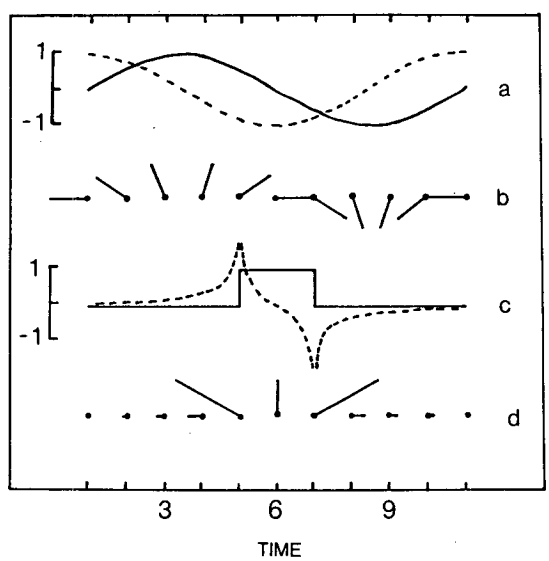

FIG. 1. (a) Sine function [solid line; $u(t) = \sin 2\pi(t-1)/10$] and its Hilbert transform [dashed line; $\hat{u}(t) = \cos 2\pi(t-1)/10$] for $1 \leq t \leq 11$. (b) The complex time series $U(t) = u(t) + i\hat{u}(t)$ plotted from $t = 1$ to $t = 11$. Each element of the time series is plotted in a vectorial format where its amplitude is indicated by the length of the vector and its phase is arranged analogously to the hour hand of a clock. The real part $u(t)$ is oriented from top to bottom; the imaginary part $\hat{u}(t)$ is oriented from left to right. (c) Pulse [solid line; $u(t) = 1$ for $5.01 \leq t \leq 6.99$; $u(t) = 0$ for $t < 5.01$ and $t > 6.99$] and its Hilbert transform {dashed line; $\hat{u}(t) = \pi^{-1}\ln[(6.99 - t)/(5.01 - t)]$ for $t < 5.01$; $\hat{u}(t) = \pi^{-1}\ln[(6.99 - t)/(t - 5.01)]$ for $5.01 \leq t \leq 6.99$; $\hat{u}(t) = \pi^{-1}\ln[(t - 6.99)/(t - 5.01)]$ for $t > 6.99$]}. (d) As in (b) but for the pulse.

The form of the Hilbert transform of the pulse in Fig. 1c is less obvious; $\hat{u}(t)$ is largest near the onset and demise of the pulse. Even though they affect only the phase of a time series when considered over its entire length, Hilbert transforms may have undesirable properties at particular times. In the case of a pulse, the amplitude of $U(t)$ in Fig. 1d is larger at the edge of the pulse than it is in the center. This leads to an important property of CPC analysis: since correlations between time series are heavily weighted by periods during which the amplitudes of the time series are large, more weight is given to sharp transitions and noisy spikes than to periods during which the signal varies slowly. Stated another way, the Hilbert transform does not act as a low-pass filter upon the data; it contains as much energy due to noise as the original data and it may redistribute the noise to different parts of the time series. In order to minimize this problem, the filter weights $W(\omega)$ can be chosen so as to apply a low-pass filter to both the original data and its Hilbert transform prior to further computations.

b. Computation of principal components and eigenvectors

For the purposes of later transformations, it is more straightforward to describe CPC analysis in terms of correlation matrices than in terms of covariance matrices. (The relative merits of covariance and correlation matrices in principal component analysis are discussed by Kutzbach, 1970.) If the complex observations $U_j(t)$ are converted into normalized anomalies by subtracting the mean and dividing by the standard deviation at each spatial position, then the correlation between the jth and kth position is

$$r_{jk} = [U_j(t)^* U_k(t)]_t, \quad (5)$$

where the asterisk denotes complex conjugation and $[\cdots]_t$ indicates a time average. The CPC approach compresses the information contained in the correlation matrix into a relatively few complex eigenvectors with elements e_{jn} and complex principal components $P_n(t)$. Since the correlation matrix is Hermitian, it possesses real eigenvalues λ_n.

The observation $U_j(t)$ can be represented as a sum of the contributions from the N principal components:

$$U_j(t) = \sum_{n=1}^{N} e^*_{jn} P_n(t). \quad (6)$$

The complex principal components, like the original time series, are normalized, i.e. $\langle P_n(t)^* P_m(t) \rangle_t = \delta_{nm}$, and the complex eigenvectors are orthogonal $\langle e^*_{jn} e_{jm} \rangle_j = \lambda_n \delta_{nm}$. An element, e_{jn}, of the nth complex eigenvector can be interpreted as

$$e_{jn} = [U_j(t)^* P_n(t)]_t = s_{jn} e^{i\theta_{jn}}. \quad (7)$$

Hence e_{jn} is the complex correlation between the jth time series and nth principal component where s_{jn} is the magnitude of the correlation and θ_{jn} is the phase. The elements of the principal component time series can also be written in terms of an amplitude T_n and phase ϕ_n, i.e. $P_n(t) = T_n(t) e^{i\phi_n(t)}$ and can be plotted as in Fig. 1b.

An alternative approach to the above would be to compute the correlations between all pairs of spatial maps rather than between all pairs of time series. Complex principal component analysis of such correlation matrices would result in principal components that are spatial maps and eigenvectors that are time series. This approach is recommended when the number of independent time steps is fewer than the number of independent grid points.

The phases θ_{jn} and $\phi_n(t)$ are known only to within an additive constant. In the case of real principal components, the additive constant is either 0 or π; i.e. the sign of the principal components is ambiguous. However for complex principal components, the constants can be within the entire range from 0 to 2π. This indeterminancy becomes important when the researcher wishes to compare complex principal components obtained from independent data sets (e.g. zonal wind to rainfall or sea surface temperature). In such cases, it is impossible to determine lead–lag relationships between the independent complex principal components by simply computing their cross-correlation since the phase of each complex principal component is known only to within an arbitrary constant. This problem can be avoided by including all relevant data into one unambiguous analysis.

When solutions of the form of (2) are assumed in linear wave dynamics, it is expected that at the end of the analysis only the real part of the solution will be considered. However, the real and imaginary parts of complex principal components are not Hilbert transforms of one another. They do not necessarily explain the same amount of variance in each frequency band and thus the real part of the complex principal components does not contain all the relevant information. Frequency domain principal component analysis does not suffer from this problem because in that approach the principal component is a real time series (see Michaelson, 1982; or Brillinger, 1981, pg. 345).

It is possible to reconstruct the portion of each complex time series that is explained by the nth component:

$$U'_j(t) = e^*_{jn} P_n(t). \quad (8)$$

The real and imaginary parts of $U'_j(t)$ are Hilbert transforms of one another and, in theory, the real part can be considered alone. In practice, the real part of $U'_j(t)$ may be misleading at grid points that are poorly explained by the complex principal component. This point is discussed further in Section 3.

c. *Linear transformation (rotation) of complex principal components*

In some cases, it may be known beforehand that principal component analysis will not yield the sort of information that the researcher desires. This is often the situation when strong regional relationships within large data sets are expected, since the principal component solution emphasizes domain-sensitive and predictable geometric patterns. There are a variety of solutions to this potential problem, e.g. varimax, quartimax, promax, oblimax (Horel, 1981; Richman, 1981) which identify regional relationships from the principal component solution. In this section, a generalization of the varimax technique to encompass CPCs is described.

An estimate $U'_j(t)$ of the observation $U_j(t)$ can be reconstructed from the first N' CPCs where $N' \ll N$ and N is the total number of CPCs:

$$U'_j(t) = \sum_{n=1}^{N'} e^*_{jn} P_n(t). \quad (9)$$

The choice of the number of components N' to retain in the estimate of $U_j(t)$ remains one of the important considerations in any transformation. Generally, more components should be retained than those determined from the significance tests of Barnett and Preisendorfer (1978), Overland and Preisendorfer (1982) or North *et al.* (1982) so that all the relevant information is retained within the estimate $U'_j(t)$. The Guttman lower bound criterion is used in this paper (Guttman, 1954; Hakstian *et al.*, 1982). It recommends retaining all of the principal components that contribute more total variance than does the typical normalized time series, i.e. one unit of total variance. Richman (1981) notes that it is safer to choose too many components than to choose fewer components than are suggested by such criteria. Hakstian *et al.* (1982) suggest applying several criteria, including the Guttman criterion, in order to choose the optimum number of components.

The estimate $U'_j(t)$ can be described in terms of the transformed solution as

$$U'_j(t) = \sum_{m=1}^{N'} g^*_{jm} F_m(t), \quad (10)$$

where $F_m(t)$ is an element of the mth rotated complex principal component (RCPC) and g_{jm} is the complex correlation (loading) between the mth RCPC and the jth observation $U_j'(t)$.

In principal component analysis, the total amount of variance explained by the first PC is maximized:

$$\lambda_1 = \sum_{j=1}^{J} e_{j1}^2 \tag{11}$$

where e_{j1} is the (real) correlation between the jth time series and the first principal component. Similarly, CPC analysis maximizes

$$\lambda_1 = \sum_{j=1}^{J} e_{j1}^* e_{j1}, \tag{12}$$

where e_{j1} is a complex correlation and e_{j1}^* is its complex conjugate. In other words, CPC analysis maximizes the sum of the squares of the amplitudes of the correlation coefficients between the first CPC and the original time series. Maximizing a first-moment statistic causes the correlation coefficients to be poorly distributed, (i.e. many loadings with magnitudes between 0.4 and 0.6) resulting in spatial patterns which, as the following will indicate, are often difficult to interpret.

The correlation between two grid points r_{jk} [see (5)] can be written in terms of the contributions from each of the CPCs as

$$r_{jk} = \sum_{n=1}^{N} e_{jn} e_{kn}^*. \tag{13}$$

If the magnitudes of the correlation coefficients e_{j1} and e_{k1}^* are large (0.7–0.9) then only the first CPC is needed to interpret the relationship between the time series at grid points j and k. However, if their magnitudes are smaller (0.4–0.6), then more than one CPC must be considered since the first CPC only explains a small fraction of the variance at each grid point (16–36%). In many instances, the first CPC may indicate a strong in-phase relationship between the time series at grid points j and k while the second one indicates a weaker, out-of-phase relationship. These types of situations often result from the usually undesirable constraint that the eigenvectors be orthogonal.

Rather than maximizing a first moment statistic (the sum) of the squared correlation coefficients, the varimax method maximizes a second moment statistic (the variance). Maximizing a second moment statistic causes the loadings of the RCPCs to be widely distributed with a few large loadings and many close to zero. Hence, in large data sets, strong regional relationships between variables are emphasized at the expense of marginal ones that encompass the entire domain. The effectiveness of the rotation depends on the degree to which distinct regional features exist within the data set.

For the case of real principal components, the varimax technique maximizes:

$$\sigma_1^2 = \frac{1}{J} \sum_{j=1}^{J} \left(\frac{g_{j1}^2}{h_j^2} - \sum_{j=1}^{J} \frac{g_{j1}^2}{J h_j^2} \right)^2, \tag{14}$$

where h_j^2 is a normalizing factor and represents the portion of the variance of the jth time series explained by all N' factors:

$$h_j^2 = \sum_{n=1}^{N'} e_{jn}^2. \tag{15}$$

By analogy for complex principal components, the following quantity is maximized:

$$\sigma_1^2 = \frac{1}{J} \sum_{j=1}^{J} \left(\frac{g_{j1}^* g_{j1}}{h_j h_j^*} - \sum_{j=1}^{J} \frac{g_{j1}^* g_{j1}}{J h_j h_j^*} \right)^2. \tag{16}$$

This requires only minor modifications to the widely available varimax subroutines. In the IMSL (International Mathematical and Statistical Library) package version, terms such as $2xy$ and $x^2 - y^2$ should be replaced by $xy^* + x^*y$ and $xx^* - yy^*$ respectively. A listing of all routines required for CPC analysis is available from the author.] Notice that all of these criteria depend only on the amplitudes of the loadings, not on the phases. In order to maximize (16), the complex loadings g_{jm} are expressed in terms of the complex eigenvectors e_{jn}:

$$g_{jm} = \sum_{n=1}^{N'} t_{mn} e_{jn}, \tag{17}$$

where the coefficients t_{mn} of the transformation matrix $\mathbf{T}$ are real. The coefficient t_{mn} can be interpreted as the correlation between the nth CPC and the mth RCPC. The transformation matrix $\mathbf{T}$ is determined iteratively until equations of the form of (16) are maximized for each of the remaining RCPCs, i.e.

$$\sigma^2 = \sum_{n=1}^{N'} \sigma_\wedge^2. \tag{18}$$

Kaiser (1958) indicates that σ^2 can not exceed $(N' - 1)/N'$. The diagnostic

$$\nu = 100\sigma^2 N'/(N' - 1) \tag{19}$$

can be used to estimate the effectiveness of the varimax transformation. If ν is large (experience from a limited number of cases suggests values in excess of 60), then the transformation efficiently describes regional factors which are nearly orthogonal; if ν is small (less than 40), then the varimax approach is inappropriate because the data set cannot be effectively described in terms of regional orthogonal factors.

The basic properties of orthogonally rotated principal components listed by Horel (1981) apply as well to RCPCs. The following are especially important:

1) RCPCs are temporally orthogonal; thus the fractions of normalized variance that they explain are additive.

2) The loading vectors of RCPCs are not constrained to be spatially orthogonal. The loading vectors of the RCPCs are less likely to be members of a family of predictable geometric patterns than are the complex eigenvectors of the CPCs.

3) The rotated solution is less dependent on the domain of the analysis. A RCPC which describes the variability of the equatorial wind field should be evident whether the domain is an equatorial band or the entire tropical wind field.

4) The RCPC solution is only one of an infinity of alternative solutions which can be derived from the CPCs. However, all of the readily available alternative solutions are designed to satisfy the simple structure criterion of L. L. Thurstone (see Harman, 1967, p. 98). As with any statistical tool, the researcher must determine whether the statistical results have any physical meaning.

3. Examples

A variety of simple examples were analyzed using the CPC technique. Combinations of propagating and standing functions at different frequencies and wavenumbers were investigated on a small array of 11 grid points oriented along a line. The techniques and results are completely applicable to two- or three-dimensional fields of larger size.

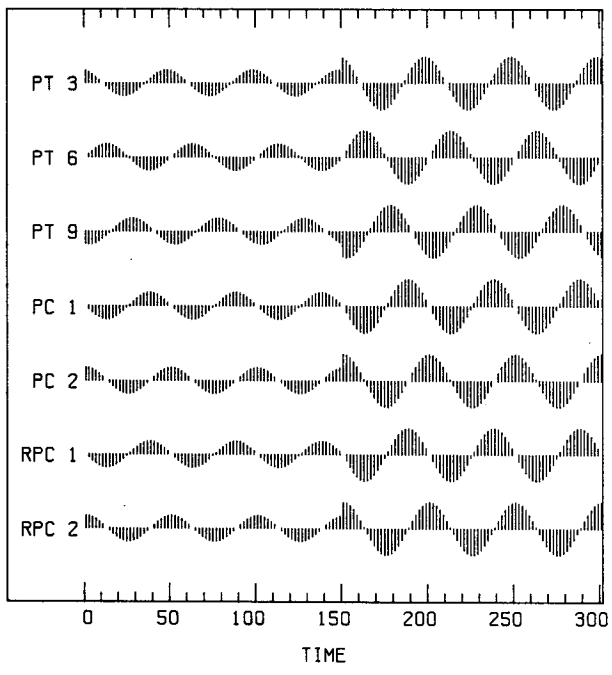

FIG. 2. Selected time series derived from principal component analysis of Example 1. Rows 1–3: $u_j(t)$ at the third, sixth, and ninth grid points. Rows 4–5: first and second principal components. Rows 6–7: first and second rotated principal components. Each element of the time series is plotted in a vectorial format where the amplitude is indicated by the length of the vector and the sign is indicated by the direction (up is positive, down negative).

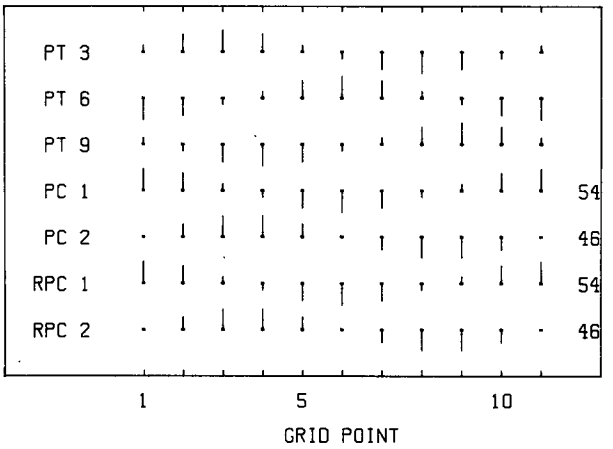

FIG. 3. Correlations between the selected time series shown in Fig. 2 and the time series at each of the 11 grid points derived from Example 1. Each correlation is plotted in a vectorial format where the magnitude of the correlation is indicated by the length of the vector and the sign is indicated by the direction (up—positive correlation, down—negative correlation). Full scale (correlation equal to 1.0) is indicated by the correlation between point 3 and itself. The numbers in the right margin are the percent of variance (λ_n 100/11) explained by the time series indicated in the left margin. They are rounded to the nearest integer.

a. Example 1

Consider the case of sinusoidal waves that move from left to right across the array of 11 grid points and their amplitude $A(t)$ as a function of time (i.e. the time series are nonstationary):

$$\textit{Example 1:}\quad u_j(t) = A(t)\sin 2\pi\left(\frac{j-1}{10} - \frac{t-1}{50}\right), \quad (20)$$

where $1 \leqslant j \leqslant 11$; $1 \leqslant t \leqslant 301$; $A(t) = 1$ for $t \leqslant 150$; $A(t) = 2$ for $t > 150$.

For the purposes of comparison, we first analyzed this example using conventional PC analysis. Figure 2 shows the time series of $u_j(t)$ at the third, sixth, and ninth grid points. The progression of the waves is clearly evident; the crest of the wave located at point 3 at time 47.5 moves to point 6 by time 62.5 and reaches point 9 at time 77.5. The doubling of the amplitude of the time series is clearly evident starting at time step 151. The correlations between the time series at grid points 3, 6, and 9 and each of the other grid point time series are shown in Fig. 3. For example, point 3 is positively correlated with its neighbors and negatively correlated with the points a half wavelength away.

The first and second principal components (which together explain 100% of the total variance) are shown in Fig. 2; their eigenvectors in Fig. 3. As should be expected, PC analysis decomposes the traveling wave into two standing waves in quadrature with one another. The PC analysis has no trouble in handling the nonstationarity of the time series. Since the initial solution also satisfies the varimax criterion of (14), the rotated principal components and principal components shown in Fig. 2 and their spatial patterns in Fig. 3 are identical. The diagnostic v from (19) has a value of 54, which indicates moderate success by the varimax transformation in describing regional features within the data set.

Figures 4 and 5 show the results of CPC analysis applied to Example 1. The sine wave was augmented by its Hilbert transform (in this case, a cosine wave of the same wavenumber and temporal frequency) according to the techniques described in Section 2a in order to form the complex time series $U_j(t)$. The first and last 30 time steps of $U_j(t)$ were tapered using a portion of a cosine bell distribution to minimize end effects. Figure 4 shows the complex time series at the third, sixth, and ninth grid points. Each element of the complex time series is depicted in the vectorial format used in Figs. 1b and 1d. The progression of the waves is clearly evident in Fig. 4. Note that the abrupt jump in the amplitude between time steps 150 and 151 creates an abrupt change in the Hilbert transform (this change is also discussed regarding Figs. 1c and 1d). Figure 5 shows the complex correlations between the time series at grid points 3, 6 and 9 and each of the other grid point time series. The

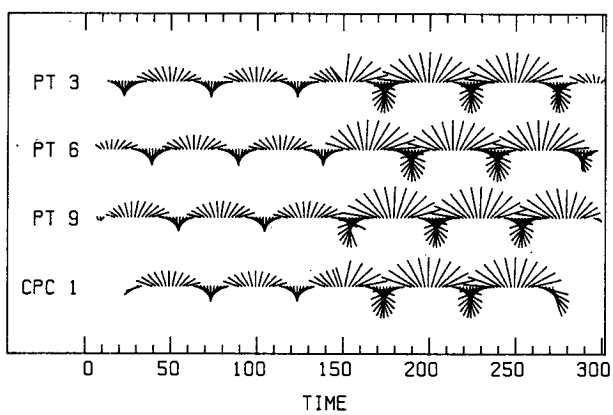

FIG. 4. Selected time series derived from complex principal component analysis of Example 1. Each complex element of the time series $[u_j(t), \hat{u}_j(t)]$ is plotted in a vectorial format where the amplitude is indicated by the length of the vector and the phase is arranged like the hour hand of a clock. To conform with the perspective derived from viewing real time series, the real part $u_j(t)$ is oriented from top to bottom while the imaginary part $\hat{u}_j(t)$ is oriented from left to right. To reduce the clutter of the figure, the vectors of even-numbered time steps and vectors whose real parts were less than ±0.1 were omitted.

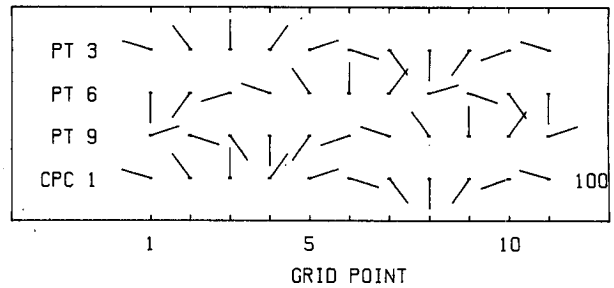

FIG. 5. Complex correlations between the complex time series shown in Fig. 4 and the complex time series at each of the 11 grid points derived from Example 1. Each complex correlation is plotted in a vectorial format where the magnitude is indicated by the length of the vector and the phase is arranged like the hour hand of a clock. A vector pointing upwards (downwards) indicates that the two time series are in-phase (out-of-phase); one pointing to the right (left) indicates that the grid point time series lags (leads) the time series indicated in the left margin by 90°; etc. The numbers in the right margin are the percent of variance explained by the time series indicated in the left margin. They are rounded to the nearest integer.

first and last 30 time steps were omitted from the computations of the correlation matrix and its eigenvectors. The correlations between point 3 and the other time series delineate the propagation of the sinusoidal waves across the domain: points 1 and 2 are perfectly correlated with point 3 and lead it by 72 and 36° respectively; point 3 is perfectly related with itself while it leads the points to its right in increments of 36°. Identical relationships are observed between points 6 and 9 and the other time series.

The first CPC (which explains 100% of the total variance) is shown in Fig. 4; its eigenvector is shown in Fig. 5. The CPC analysis has correctly identified the temporal frequency and wavenumber of the sinusoidal waves and correctly identified the change in amplitude of the waves near time step 151. The eigenvector in Fig. 5 indicates that the CPC is perfectly correlated with each of the original time series. Since the CPC explains all of the variance, there is no need to seek alternative solutions.

The phase of the CPC is known only to within an additive constant; hence only the relative phase relationships exhibited in the eigenvector can be considered, e.g. grid point 6 lags (leads) grid point 3 (9) by 108°. An arbitrary convention was adopted that the element of the first eigenvector with the largest amplitude points up. The temporal and spatial distributions of the CPC and its eigenvector can be used to convert the relative phase in degrees into a more meaningful measure. For example, the number of time steps between successive peaks of the CPC in Fig. 4 (1 cycle per 50 time steps) and the wavenumber of the eigenvector in Fig. 5 (1 cycle per 10 grid points) indicates that the phase speed of the traveling waves is 0.20 grid points per time step. Hence, grid

point 3 leads grid point 6 by 15 time steps as can be verified by inspection of the top two rows of Fig. 4.

b. Example 2

One of the common concerns regarding CPC analysis is that it will decompose standing oscillations into retrogressive and progressive components in much the same manner that conventional principal component analysis decomposes traveling waves into standing oscillations. This example represents a superposition of standing waves and eastward-traveling waves in order to show the ability of CPC analysis to differentiate between these phenomena:

$$\textit{Example 2:}\quad u_j(t) = \sin 2\pi\left(\frac{j-1}{5} - \frac{t-1}{30}\right) + \sin 2\pi\left(\frac{j-1}{10}\right)\sin 2\pi\left(\frac{t-1}{60}\right). \quad (21)$$

For simplicity, in this and all of the following examples, the amplitudes of the input waves are constant with time. Figures 6 and 7 show selected time series and correlations respectively for this case. In Fig. 6, the time series at points 3, 6, and 9 delineate the superposition of the traveling waves upon the lower frequency standing waves. The correlations in Fig. 7 between points 3, 6 and 9 and the other points would be difficult to interpret by themselves; for example, nearby points are well correlated with point 3 but point 8 is completely unrelated to it. Complex principal component analysis in this case conveniently

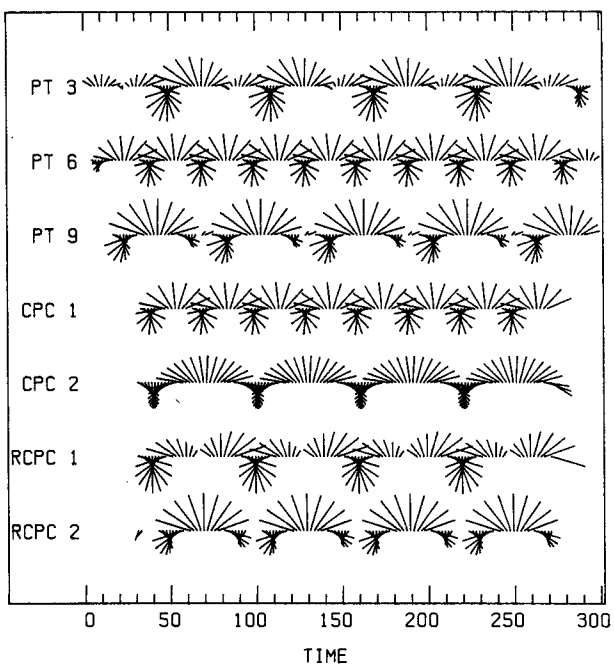

FIG. 6. As in Fig. 4 but for Example 2.

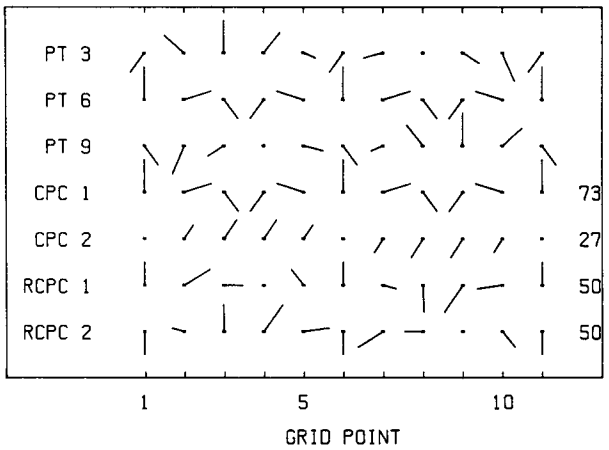

FIG. 7. As in Fig. 5 but for Example 2.

simplifies the interpretation by separating the traveling waves (CPC 1) from the standing waves (CPC 2) as shown by their distinctive temporal frequencies in Fig. 6 and spatial distributions in Fig. 7. Note that the traveling wave explains more variance simply because the standing wave has no amplitude at points 1, 6, and 11.

The linear transformations of the CPCs according to the varimax criterion for this case are also shown in Figs. 6 and 7. This example illustrates the type of phenomenon that is ill-suited for varimax transformations. The value of ν from (19) is 30. In this instance, further analysis has not helped because the first RCPC essentially describes the variations near the right antinode of the standing oscillation while the second one describes the variations near the left antinode. In cases such as this one where the waves encompass the entire domain, the varimax criterion is not particularly useful.

c. Example 3

In many geophysical applications, the domain of the analysis is much larger than the scale of the phenomenon to be investigated. Consider the following case in which sinusoidal waves in the left-hand half of the domain travel from left to right while other waves in the right-hand half of the domain travel from right to left:

Example 3:

$$\left.\begin{aligned} u_j(t) &= \sin 2\pi\left(\frac{j-1}{5} - \frac{t-1}{50}\right), \quad 1 \leq j \leq 6 \\ u_j(t) &= \sin 2\pi\left(\frac{j-1}{5} + \frac{t-1}{60}\right), \quad 6 < j \leq 11 \end{aligned}\right\}. \quad (22)$$

Figure 8 shows time series for this case; Fig. 9 shows correlations. The simple wave structure at points 3

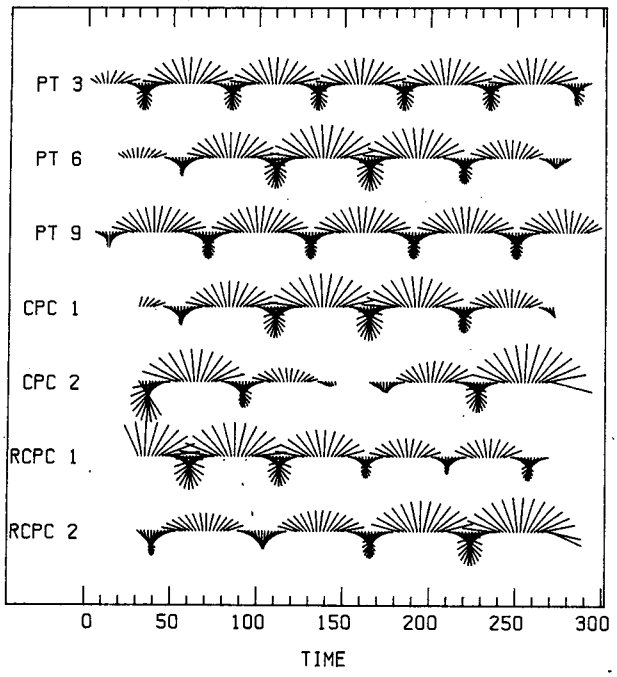

FIG. 8. As in Fig. 4 but for Example 3.

and 9 is clearly evident in Fig. 8 while the superposition of the two types of waves at point 6 results in more complicated temporal variability. The correlations between point 3 and the other time series indicate the rightward-traveling waves in the left-hand portion of the domain and no relationship with the variations in the other half of the domain; similarly, the change of phase of the correlations between point 9 and the other time series indicate that the leftward-moving waves are in the right-hand portion of the domain.

The complex eigenvectors for this case are shown in Fig. 9. The basic tendency for CPCs to describe domain-wide spatial patterns (even when no such patterns exist in the data set) is evident. The first CPC describes primarily the variations at point 6 where the two types of waves overlap. The second CPC clearly results from the constraint that its spatial pattern be spatially orthogonal to the first one. Both principal components must be considered in order to recognize that no relationship exists between the right and left halves of the domain [see (13)].

Transformation of the CPCs according to the varimax criterion simplifies the interpretation by emphasizing the large correlations observed in the two halves of the domain. The first RCPC describes the traveling waves in the left-half of the domain while the second describes those in the right half. The diagnostic ν has a value of 65 in this instance; this value indicates that the transformation successfully identifies regional features within the data set.

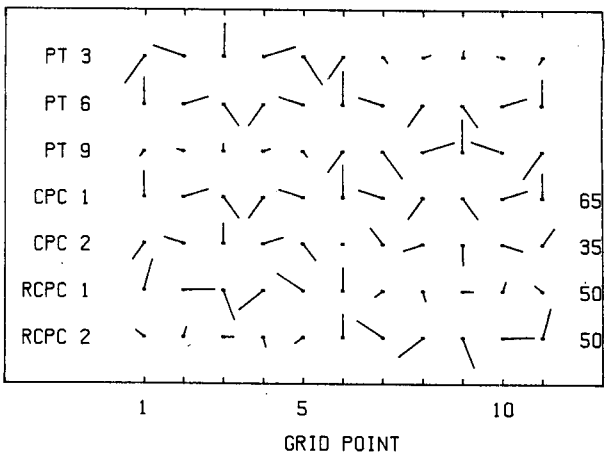

FIG. 9. As in Fig. 5 but for Example 3.

d. Example 4

As mentioned in the Introduction, many geophysical phenomena involve progressive waves which occur at irregular intervals. Consider the following case in which short duration events move from left to right across the domain:

$$\textit{Example 4:}\quad u_j(t) = \sum_{i=1}^{6} \exp - 0.25[2(j-1) - (t-t_i)]^2 + \exp - 0.25[2(j-1) - (t-t_i')]^2, \quad (23)$$

where $t_i = 5.0\epsilon + 40i$, $t_i' = 20 + 40i + 5.0\epsilon'$, ϵ and ϵ' are random numbers. Figure 10 shows the normalized

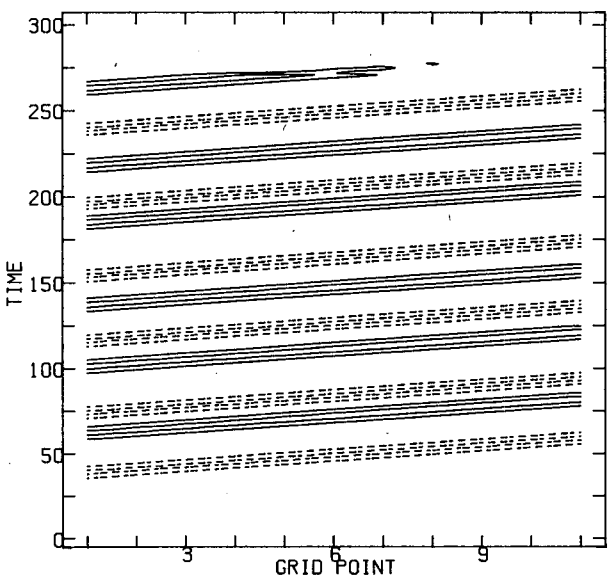

FIG. 10. Normalized anomalies $[u_j(t)]$ generated from the equations of Example 4. Positive anomalies are indicated by solid contours; negative anomalies by dashed contours; the zero line is omitted. Contour interval is 1.0 standard deviation.

anomalies generated by these equations. The propagation of each positive and negative anomaly pulse is clearly evident.

Figures 11 and 12 show the results of CPC analysis applied to Example 4. Consider first the spatial behavior of the solution. According to the complex correlations in Fig. 12, the time series at the three points demonstrate strong coherence with nearby time series but fail to have strong correlations with the time series at points farther away. The first CPC does not explain all of the variance, even though there is a very obvious signal in the original data set. The first eigenvector in Fig. 12 shows the left-to-right progression of the pulses, giving slightly more weight to the grid points near the center of the domain than to those near the edges. The second CPC clearly explains a residual of the total variance and has little physical meaning. The first RCPC emphasizes more heavily the signal in the center of the domain; since ν equals 20 in this case, the rotated solution should not be given much weight.

The complex time series of the three grid points in Fig. 11 indicate the relatively short duration and progression of each event. Although it may be difficult to notice in the figure, the pulses of the first CPC are broader than those in the original data (more vectors of the first CPC point up than those of the original time series). The temporal behavior of the first RCPC more closely resembles that of the time series at grid points 5 and 6.

The first CPC does not explain all of the variance in this example because of the nature of the data.

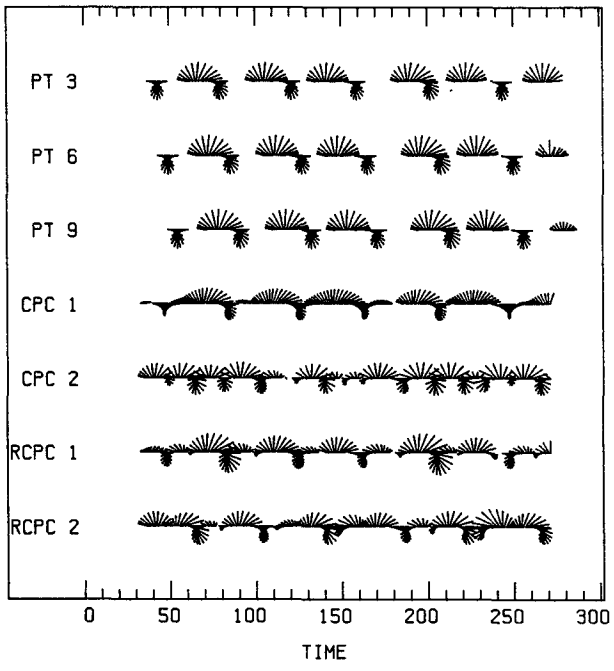

FIG. 11. As in Fig. 4 but for Example 4. All vectors are plotted.

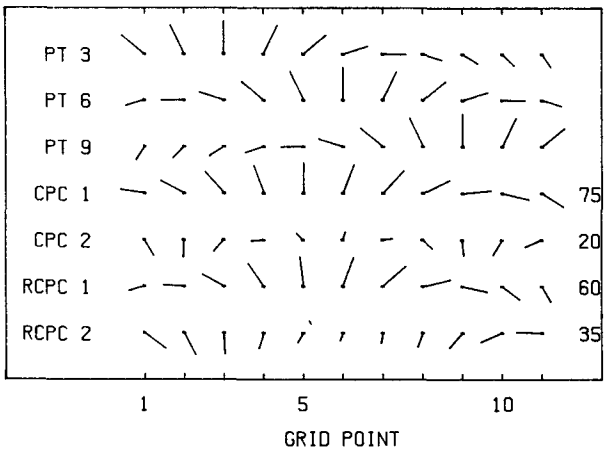

FIG. 12. As in Fig. 5 but for Example 4.

Imagine computing the complex correlation between gridpoint 1 and 11 on the basis of the real parts of the time series shown in Fig. 10. At time step 200, the two time series are out of phase while at time step 100, there is no relationship at all since the real part of gridpoint 11 is zero. Hence the complex correlation between grid point 1 and 11 depends strongly on the phase speed, duration, and spacing of each pulse. In this example, the duration of each pulse at any particular point (roughly five time steps) is relatively short in comparison to the time it takes for the pulse to travel across the domain (20 time steps). If the pulses travel at relatively slow phase speeds, then the relationships between distant points become tenuous, unless the phenomena is nearly periodic. In other words, one should not expect to be able to detect slow moving, irregularly spaced pulses over vast distances accurately on the basis of complex correlations. The complex principal components will approximate the proper solution but they may differ from the proper solution in some respects in order to satisfy constraints of the analysis approach.

The portion of the data explained by the first CPC was reconstructed using (8) and its real part is shown in Fig. 13. The reconstruction exhibits several features which differ from those of the original data shown in Fig. 10: the amplitude of each pulse is generally weaker, the duration of each pulse is slightly longer, and spurious events appear at the edges of the domain. The reason for these discrepancies is that the first CPC represents a combination of the original complex time series with more weight given to the variability near the center of the domain than to that at the edges (see Fig. 12). Since the first CPC is in quadrature with the time series near the edges, the reconstruction near the edges is due partially to the imaginary portion of the time series near the center of the domain. The correlation between the reconstruction based on the nth CPC and the original time series is

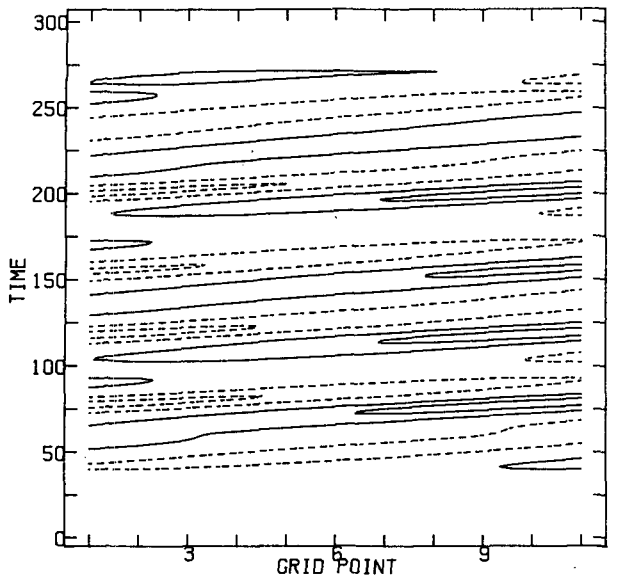

FIG. 13. Reconstruction according to (8) of the normalized anomalies of Example 4 from the first CPC. Plotting as in Fig. 10.

$e_{jn}e^*_{jn}$. Since the time series near the edges contribute less to the first RCPC, the reconstruction based on the first RCPC is even more inaccurate near the edges and more accurate in the center of the domain (not shown). The regions of a reconstruction which are poorly explained by a complex principal component should be clearly delineated.

Many other cases of propagating and standing wave behavior were examined. For example, cases in which progressive pulses traveled from left to right in one-half of the domain while others traveled from right to left in the other half of the domain (i.e. a combination of the features of Examples 3 and 4) indicated that the RCPCs can correctly identify regional pulses while the CPCs cannot. The diagnostic ν in these instances was greater than 60.

RCPCs of the equatorial wind field analyzed by Barnett (1983) were also calculated. The first RCPC explained slightly more variability of the zonal wind in the central equatorial Pacific with less emphasis on changes in the Indian Ocean. In this case, ν equalled 52 and hence the RCPC solution is marginally useful.

4. Sampling Errors

The results obtained in the preceding section would not have changed if other data samples had been chosen from the populations defined by (20–23). However, as discussed by North *et al.* (1982), errors in PC analysis arising from limited sample sizes should be of more concern than has been evident in recent literature. Physical significance has been attached all too frequently to principal components that are unreproducible in independent data sets. The sampling errors of complex eigenvectors and principal components are determined in a fashion analogous to that used in PC analysis as shown by Brillinger (1981, pp. 340–343). Assuming that the sample estimate of the population covariance matrix has a complex Wishart distribution, then the asymptotic limit of the standard error of the nth eigenvalue is

$$l_n = \lambda_n\left(\frac{1}{\tau}\right)^{1/2}, \tag{24}$$

where τ is the number of independent time steps. Note that the standard error for the eigenvalues of real covariance matrices is $\sqrt{2}$ larger because the complex time series have twice as many degrees of freedom (Brillinger, 1981).

The contribution, $\eta_n(j)$, to the sampling error of the jth element of the nth eigenvector e_{jn} resulting from the next eigenvector is, according to Brillinger (1981),

$$\eta_n(j) = \left(\frac{\lambda_n\lambda_{n+1}}{\tau}\right)^{1/2}\frac{s_{jn+1}}{\lambda_{n+1}-\lambda_n}, \tag{25}$$

where s_{jn+1} is the magnitude of e_{jn+1}. Although (25) is in a slightly different form than that shown by North *et al.* (1982), its interpretation is the same: i.e. when successive eigenvalues are close to one another, then the sampling error of the complex eigenvector is large. In other words, if two principal components explain nearly the same variance, then the researcher can have little confidence that another sample will yield the same principal components; instead a myriad of linear combinations of the two principal components are possible.

In some instances, successive eigenvalues can be nearly identical, yet transformation of the principal components can yield a solution which is more invariant from sample to sample. This can happen in situations where two or more regional features explain roughly the same amount of variance. Rigorous proof of the sampling errors of linear transformations of principal components is beyond the scope of this paper. Consider instead the following example based on real time series which illustrates the differences in sampling errors of unrotated and rotated principal component solutions. It applies equally well to CPC solutions.

A random time series $U_1(t)$ consisting of 3000 time steps was first generated. Time series at nine successive gridpoints were then generated according to the following:

$$U_{j+1} = \rho_{j+1}U_j(t) + (1-\rho^2_{j+1})^{1/2}\epsilon_{j+1}(t), \tag{26}$$

where ρ_{j+1} is the correlation between the $(j+1)$ and jth time series and $\epsilon_{j+1}(t)$ is a random time series with unit variance. The ten time series comprise the population data set. The correlations ρ_{j+1} were chosen

so as to have the first five time series strongly correlated with one another and uncorrelated with the last five time series, i.e. the nine values of ρ_{j+1} are 0.8, 0.8, 0.8, 0.8, 0.1, 0.8, 0.8, 0.8, 0.8.

Principal component analysis of the population data set yielded the two eigenvectors shown in the upper two lines of Fig. 14. Note that the PC solution does not hint at the strong regional relationships contained within the data set; instead the first PC suggests that all the grid points are positively correlated, while the second PC indicates that the left and right halves of the domain are inversely related. The two principal components explain nearly the same variance as shown in the right margin of Fig. 14. According to (24), the population eigenvectors are indistinct from one another, hence eigenvectors derived from samples of this population should differ considerably.

Twenty samples consisting of 300 time steps were drawn at random from the population time series. Principal component analysis of these 20 samples showed considerable variability from sample to sample. The eigenvectors derived from three samples are shown in Fig. 14. The eigenvectors of the first sample are considerably different from the population eigenvectors; the first PC shows that the first five time series are strongly related to one another while being unrelated to the last five time series, and vice versa for the second PC. The eigenvectors derived from the other two samples are qualitatively similar to the population eigenvectors yet their magnitudes are dissimilar.

Varimax transformations of the principal components derived from the population and 20 samples were also computed. The loadings between the original time series and the rotated principal components

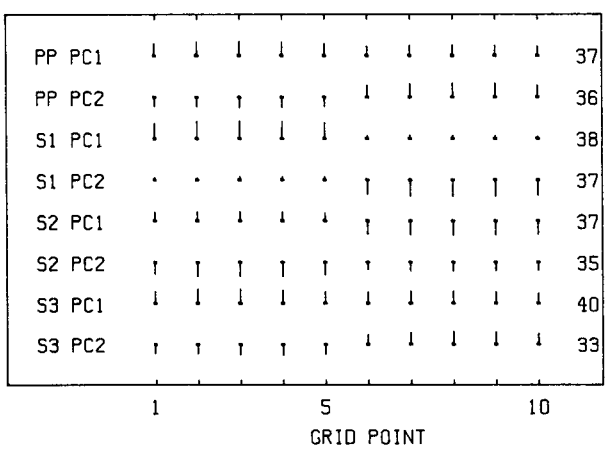

FIG. 14. Correlations between the population time series defined in Section 4 and the first and second principal components derived from the population (top two lines). Also shown are the correlations between the time series of three samples and the first and second principal components derived from the samples (S1 indicates Sample 1, etc.). Plotting as in Fig. 3.

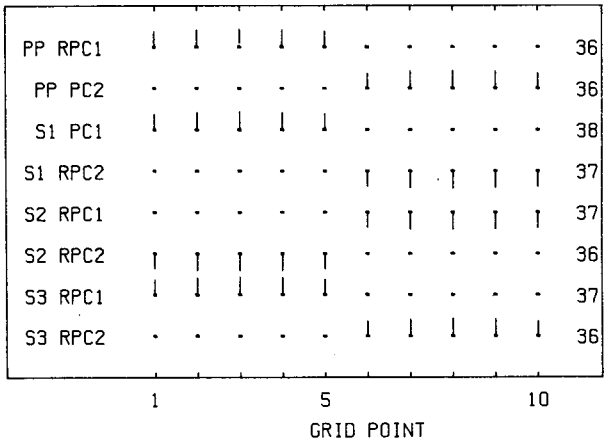

FIG. 15. As in Fig. 14 but for the correlations between the population and sample time series and the rotated principal components derived from those time series.

derived from the population and three samples used in Fig. 14 are shown in Fig. 15. The population rotated principal components emphasize the two strong regional relationships that were built into the data set. The three samples also show the same strong regional relationships, although the signs (which are completely arbitrary) of the rotated principal components vary from sample to sample. For both population and sample rotated principal components (RPC), the values of ν from (19) exceeded 95.

In order to measure quantitatively the variability from sample to sample of the principal components and rotated principal components, the root mean square difference between each pair of samples was computed:

$$ER^2(n) = \frac{1}{1900} \sum_{j=1}^{10} \sum_{y=1}^{20} \sum_{z=y+1}^{20} [|e_{jn}(y)| - |e_{jn}(z)|]^2, \quad (27)$$

where $e_{jn}(y)$ is an eigenvector or loading element for sample y. The PCs and RPCs of some samples were reordered so that the first component always explained the most variance of the third grid point. This ensured that only the sample components which explained the same features of the data were intercompared. The rms differences for the two principal components were roughly 0.21 while those of the rotated principal components were roughly 0.04. In other words, the correlations between the sample principal components and the original time series varied on average from sample to sample by 0.21 while the variability of the correlations between the sample rotated principal components and the original time series was five times less.

The preceding example indicates that the sampling errors of rotated solutions are not directly related to the sampling errors of PC solutions. More rigorous proof of this statement is being developed at this

time. The rotated solution in this instance suffers less from sampling errors because it emphasizes the strongest relationships within the data set. On the other hand, the PC solution seeks to maximize the total variance explained by each principal component. In so doing, weight is more evenly distributed between strong and marginal relationships. Since marginal relationships within the data set may vary from sample to sample, the principal components will vary as well.

5. Conclusions

It is important at this point to be able to assess what can be gained by using CPC analysis compared to other analysis approaches. The primary benefit of CPC analysis is that it allows propagating features to be detected and dissected in terms of their spatial and temporal behavior. The CPC approach efficiently reduces the data set into the fewest number of modes possible. Regional-scale propagating phenomena, if they exist within the data set, can be detected by transforming the CPC solution according to the varimax technique. By comparison, conventional PC analysis allows the detection of standing oscillations only; cross-spectral analysis provides information in wavenumber–frequency space only and hence regional or aperiodic phenomena are spread over many wavenumbers or frequencies; frequency domain principal component (FDPC) analysis works best when the dominant variability contained within the data set is concentrated in a narrow frequency band.

There are many drawbacks of CPC solutions which must be considered. CPC analysis is a mixture of principal component and cross-spectral methods and it suffers from the problems of both techniques, e.g. the principal components may not be reproducible from one sample to another if successive eigenvalues are nearly identical and information at the ends of the time series is lost. Several of its difficulties are unique or become worse compared to those of other approaches: the complex principal components and their eigenvectors are difficult to interpret in all but the simplest of cases because both amplitude and phase relationships must be considered; reconstructions of the data can be misleading in regions which are poorly explained by the complex principal components; sudden transitions and noisy spikes are emphasized unless the data is low-pass filtered prior to CPC analysis; and CPC solutions from separate analyses are difficult to compare. None of these problems are severe enough to inhibit the use of CPC analysis but the researcher must assess their severity for each data set.

The CPC analysis is ideally suited for many applications, e.g. identifying Kelvin waves in sea level records, forced Rossby waves in upper-tropospheric geopotential height fields, or climatic records of sea level pressure or wind. No matter what the application, the results of CPC analysis are difficult to interpret without supporting information. Time series (real and complex) at key locations should be plotted along with the correlations (real and complex) between the selected points and the entire data field. Of course, the best check of a complex principal component solution is whether it makes sense physically and whether it can be seen in the original data fields.

Acknowledgments. Interest in this area of research was generated by the CPC studies performed by T. P. Barnett, Climate Research Group. He generously provided most of the analysis routines and greatly improved the study with his comments and suggestions. Thanks are also due to R. Mendelssohn, Southwest Fishery Center; G. Philander, Geophysical Fluid Dynamics Laboratory and Michael Richman, Illinois State Water Survey, for their suggestions and comments. This research was supported by the Mellon Foundation and NSF Grant ATM83-00474 of the Climate Dynamics Program.

REFERENCES

Anderson, J. R., and R. D. Rosen, 1983: The latitude–height structure of 40–50 day variations in atmospheric angular momentum. *J. Atmos. Sci.*, **40,** 1584–1591.

Barnett, T. P., 1977: The principal time and space scales of the Pacific trade wind field. *J. Atmos. Sci.*, **34,** 221–235.

——, 1983: Interaction of the monsoon and Pacific trade wind systems at interannual time scales. Part I: The equatorial zone. *Mon. Wea. Rev.*, **111,** 756–773.

——, 1984a: Interaction of the monsoon and Pacific trade wind systems at interannual time scales. Part II: The tropical band. *Mon. Wea. Rev.*, **112,** 2380–2387.

——, 1984b: Interaction of the monsoon and Pacific trade wind systems at interannual time scales. Part III: A partial anatomy of the Southern Oscillation. *Mon. Wea. Rev.*, **112,** 2388–2400.

——, and R. W. Preisendorfer, 1978: Multifield analog prediction of short-term climatic fluctuations using a climate state vector. *J. Atmos. Sci.*, **35,** 1771–1787.

Brillinger, D. R., 1981: *Time Series–Data Analysis and Theory.* Holden-Day, 540 pp.

Denbo, D. W., and J. S. Allen, 1984: Rotary empirical orthogonal function analysis of currents near the Oregon coast. *J. Phys. Oceanogr.*, **14,** 35–46.

Guttman, L., 1954: Some necessary conditions for common-factor analysis. *Psychometrika,* **19,** 149–161.

Hakstian, R. A., W. T. Rogers and R. B. Cattell, 1982: The behavior of number of factor rules with simulated data. *Multivar. Behav. Res.*, **17,** 193–219.

Hardy, D. M., and J. J. Walton, 1978: Principal component analysis of vector wind measurements. *J. Appl. Meteor.*, **17,** 1153–1162.

Harman, H. H., 1967: *Modern Factor Analysis.* University of Chicago Press, 474 pp.

Hayashi, Y., 1973: A method of analyzing transient waves by space-time cross spectra. *J. Appl. Meteor.*, **12,** 404–408.

——, 1979: A generalized method of resolving transient disturbances into standing and traveling waves by space-time spectral analysis. *J. Atmos. Sci.*, **36,** 1017–1029.

Hogg, N., 1977: Topographic waves along 70°W on the continental rise. *J. Mar. Res.*, **39,** 627–649.

Horel, J. D., 1981: A rotated principal component analysis of the interannual variability of the Northern Hemisphere 500 mb height field. *Mon. Wea. Rev.*, **109,** 2080–2092.

Kaiser, H. F., 1958: The varimax criterion for analytic rotation in factor analysis. *Psychometrika,* **23,** 187–200.

Kao, S. K., 1968: Governing equations and spectra for atmospheric motion and transports in frequency–wavenumber space. *J. Atmos. Sci.,* **25,** 32–38.

Kundu, P. K., and J. S. Allan, 1976: Some three-dimensional characteristics of low-frequency current fluctuations near the Oregon coast. *J. Phys. Oceanogr.,* **6,** 181–199.

Kutzbach, J. E., 1967: Empirical eigenvectors of sea level pressure, surface temperature and precipitation complexes over North America. *J. Appl. Meteor.,* **6,** 791–802.

——, 1970: Large-scale features of monthly mean Northern Hemisphere anomaly maps of sea level pressure. *Mon. Wea. Rev.,* **98,** 708–716.

Legler, D. M., 1983: Empirical orthogonal function analysis of wind vectors over the tropical Pacific region. *Bull. Amer. Meteor. Soc.,* **64,** 234–241.

Madden, R. A., and P. R. Julian, 1971: Detection of a 40–50 day oscillation in the zonal wind in the tropical Pacific. *J. Atmos. Sci.,* **28,** 702–708.

Michaelson, J., 1982: A statistical study of large-scale, long-period variability in North Pacific sea surface temperature anomalies. *J. Phys. Oceanogr.,* **12,** 694–703.

North, G. R., T. L. Bell, R. F. Cahalan and F. J. Moeng, 1982: Sampling errors in the estimation of empirical orthogonal functions. *Mon. Wea. Rev.,* **110,** 699–706.

Overland, J. E., and R. W. Preisendorfer, 1982: A significance test for principal components applied to a cyclone climatology. *Mon. Wea. Rev.,* **110,** 1–4.

Preisendorfer, R. W., F. W. Zwiers and T. P. Barnett, 1981: Foundations of principal component selection rules. SIO Ref. Ser., 81-4, Scripps Institution of Oceanography, 192 pp.

Rasmusson, E. M., P. A. Arkin, W. Y. Chen and J. B. Jalickee, 1981: Biennial variations in surface temperature over the United States as revealed by singular decomposition. *Mon. Wea. Rev.,* **109,** 181–192.

Richman, M. B., 1981: Obliquely rotated principal components: An improved meteorological map typing technique. *J. Appl. Meteor.,* **20,** 1145–1159.

Speth, P., and R. A. Madden, 1983: Space-time spectral analyses of Northern Hemisphere geopotential heights. *J. Atmos. Sci.,* **40,** 1086–1100.

Thomas, J. B., 1969: *An Introduction to Statistical Communication Theory.* Wiley & Sons, 663 pp.

Trenberth, K. E., and W.-T. K. Shin, 1984: Quasibiennial fluctuations in sea level pressures over the Northern Hemisphere. *Mon. Wea. Rev.,* **111,** 761–777.

Venne, D. E., 1985: The horizontal structure of traveling planetary-scale waves in the upper stratosphere. *J. Atmos. Sci.,* (Submitted).

Wallace, J. M., 1972: Empirical orthogonal representation of time series in the frequency domain. Part II: Application to the study of tropical wave disturbances. *J. Appl. Meteor.,* **11,** 893–900.

——, and R. E. Dickinson, 1972: Empirical orthogonal representation of time series in the frequency domain. Part I: Theoretical considerations. *J. Appl. Meteor.,* **11,** 887–892.

Walsh, J. E., and M. B. Richman, 1981: Seasonality in the associations between surface temperatures over the United States and the North Pacific Ocean. *Mon. Wea. Rev.,* **109,** 767–783.

Wang, D.-P., and C. N. K. Moers, 1977: Long coast trapped waves off the West Coast of the United States, summer 1973. *J. Phys. Oceanogr.,* **7,** 856–864.

Weare, B. C., and J. S. Nasstrom, 1982: Examples of extended empirical orthogonal function analyses. *Mon. Wea. Rev.,* **110,** 481–485.